Amorphography—The Relationship between Amorphous and Crystalline Order. 1. The Structural Origin of Memory Effects in Polyaniline

M. Laridjani and J. P. Pouget*

Laboratoire de Physique des Solides (URAO2-CNRS), Université de Paris Sud, 91405 Orsay, France

E. M. Scherr and A. G. MacDiarmid

Department of Chemistry, University of Pennsylvania, Philadelphia, Pennsylvania 19104-6323

M. E. Jozefowicz and A. J. Epstein*

Departments of Physics and Chemistry, The Ohio State University, Columbus, Ohio 43210-1106

Received December 11, 1991

ABSTRACT: Many materials, especially polymers, have a substantial volume fraction without crystalline order. Though these regions are often termed amorphous, they frequently have specific local order. We describe and use here a method based on a non-energy-dispersive X-ray diffraction technique to obtain good quality interference functions and, by Fourier transform, radial distribution functions of the amorphous structures of polymers. We apply this approach to a family of electronic polymers of current interest, polyaniline, comparing polyaniline emeraldine base (EB-II prepared from NMP solution), polyaniline emeraldine salt (ES-II prepared by doping EB-II with HCl), and dedoped polyaniline ES-II salt. From these data, it is found that amorphous EB-II and ES-II show a local chain array resembling that exhibited by the recently determined EB-II and ES-II crystalline structures, respectively. Thus the order in "crystalline" and "amorphous" regions is locally similar but differs by the spatial range of structural correlations, a feature likely due to the amount of conformational defects. Dedoped polyaniline ES-II salt has an increased interchain disorder through a local structural order intermediate between those of amorphous EB-II and ES-II. These studies demonstrate the importance of sample history in evaluating the physical properties of polyaniline and provide a structural origin for memory effects previously reported.

I. Introduction

Determination of the local order in polymers has been the subject of extensive studies.[1] Analyses have been complicated by the presence of only partial crystallinity in many polymer systems. The study of the order in electronic polymers presents similar complexities. While the prototypical polyacetylene produced by the Shirakawa route is highly crystalline (75–90% of the scattered X-ray intensity constituting "sharp" Debye–Scherrer rings)[2-4] and remains largely crystalline even after p or n type doping,[4-6] the recently studied polyanilines[7] have only partial crystallinity ranging from near 0% to approximately 50% depending upon sample history.[8-12]

Two classes of the emeraldine form of polyaniline have been distinguished.[9,11] Emeraldine samples belonging to class II are prepared originally in the insulating nonprotonated base form. Class II emeraldine base, EB-II, ranges from amorphous up to 50% crystalline. The proposed structure of the crystalline part of EB-II[9,11] is reproduced in Figure 1. Upon protonation with HCl, class II emeraldine salt, ES-II, is formed. It can be up to 50% crystalline with the proposed structure[11] reproduced in Figure 2. Dedoping of ES-II (e.g., through washing with NH_4OH) leads to amorphous EB-II. Class I materials are formed when emeraldine salt is obtained directly from solution in the protonated form. The resulting ES-I is up to 50% crystalline with a different structure.[9,11] Deprotonation of ES-I leads to essentially amorphous EB-I. The amorphous polymer retains memory of its corresponding base or salt state. For example, protonation of amorphous EB-I or EB-II results in partially crystalline ES-I or ES-II, respectively.

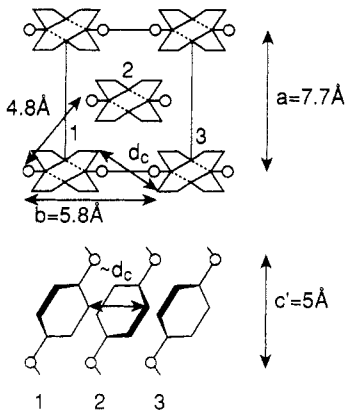

Figure 1. EB-II *Pbcn* structure of the crystalline part of undoped polyaniline, according to ref 11. Some typical distances are indicated.

It has recently been shown that the degree of order has a dramatic effect upon the electronic state of doped polyaniline (protonated emeraldine hydrochloride). For example, amorphous protonated EB-II is spinless, with its electronic structure likely in the bipolaronic form, while crystalline ES-I and ES-II have a significant Pauli susceptibility indicative of a metallic state.[9] Similarly the local order, alignment, and crystallinity have a controlling role in the conductivity of emeraldine hydrochloride[13] and of its derivatives such as poly(*o*-toluidine) hydrochloride.[14]

Local order in polyaniline also is important in electrochemical and diffusion processes. Villeret and Nechtschein[15] have reported a hysteresis or so-called "memory effect" which depends upon the electrochemical cycling[16] of polyaniline. Anderson et al. report that the diffusion

0024-9297/92/2225-4106$03.00/0

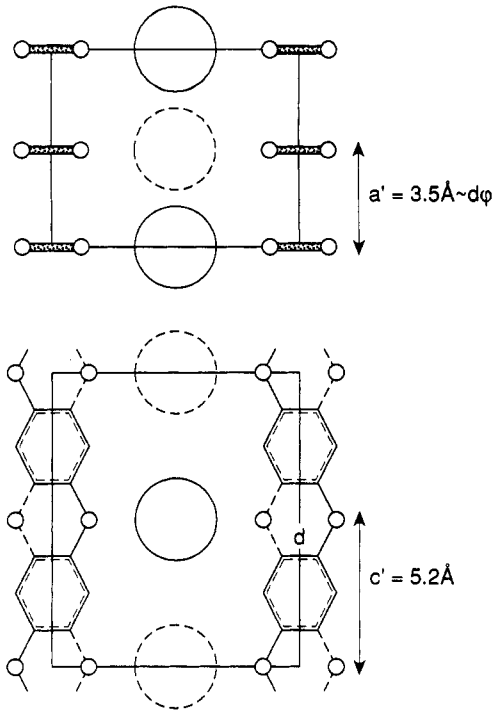

Figure 2. ES-II *Pc2a* structure of the crystalline part of HCl-doped polyaniline of type II, according to ref 11. Some typical distances are indicated.

of various gases through polyaniline membranes is dependent upon whether or not the film has ever been doped or has been doped and subsequently dedoped.[17] Similarly long-lived photoinduced optical effects[18] and magnetic effects[19] point to the important role of local conformation[20] in the polyanilines.

There are relatively few X-ray determinations of local order in amorphous polymers available in the literature.[1] This is probably due to the difficulty in obtaining good interference functions from which radial distribution functions can be derived, because organic matter weakly scatters X-rays and obtaining the coherent part of the diffracted intensity requires the subtraction of an important incoherent scattering background mainly due to Compton scattering. The elimination of this background is facilitated by the use of a non-energy-dispersive X-ray diffraction method.[21] We report here the first use of this "amorphography" technique to study the local order in polymers.

Interference functions and radial distribution functions have been determined for "amorphous" EB-II film prepared from *N*-methylpyrrolidinone solution (NMP), ES-II film prepared by equilibration of the EB-II film with pH = 0 HCl, and EB-II film after it is dedoped by washing with 1 M NH_4OH.[22,23] Our results demonstrate that the structural correlations for amorphous EB-II correspond with those expected from the EB-II[9,11] and model oligomer[24] crystal structures. After equilibration of the amorphous EB-II film with 1 M HCl, amorphous ES-II was observed. Its radial distribution function differed significantly from that of the original undoped NMP-cast, EB-II material, and its interference function shows maxima corresponding to the interchain separation determined earlier for the ES-II crystal structure.[11] Upon dedoping the ES-II to re-form amorphous EB-II, it was determined that the interference function and the radial distribution function were intermediate between those for the starting EB-II and the corresponding ES-II. These data provide direct structural evidence of a memory effect in these amorphous polymers. In particular, there is a clear difference in order between never doped amorphous EB-II and previously doped and dedoped amorphous EB-II.

In section II, the amorphography technique used to acquire the non-energy-dispersive X-ray diffraction data and the method used to derive the relevant functions obtained from these data are presented, together with the description of the preparation of polyaniline films. The interference functions and radial distribution functions obtained from the amorphous EB-II film cast from NMP, the HCl-doped film, and the dedoped film are presented in section III. These results are analyzed in the context of the proposed chain and crystal structures in section IV. Implications for physical and chemical phenomena are presented in section V. Finally, in section VI we summarize our results.

II. Experimental Section

(a) Amorphography. The implementation of amorphography requires both the experimental acquisition of appropriate diffraction data and associated analysis. The laboratory and theoretical procedures are outlined below.

(i) X-ray Technique. The record of high-quality interference functions $J(K)$ (which will be defined in the next part) was obtained by the non-energy-dispersive X-ray diffraction technique.[21] The experiment was performed at ambient conditions on a diffractometer mounted at a Ag X-ray source. Each sample was scanned from $2\theta = 2°$ to 90° in transmission geometry. The scanning step was of 0.25°, and the counting rate for large θ values was not less than 10^4 photons for each point. The scattered beam was recorded by an energy-dispersive lithium-drifted silicon detector connected with a pulse processor. The pulses are accumulated in a multichannel analyzer. With this technique a narrow energy band can be selected around the characteristic radiations of the Ag target. Both the $\lambda_{K\alpha} = 0.5609$ Å and $\lambda_{K\beta} = 0.4907$ Å wavelengths were used.

The high efficiency for the short wavelengths and the high-energy resolution of the solid-state detector (250 eV for 22 keV) permit not only the elimination of fluorescence radiation from the sample but also the partial removal of the incoherent Compton scattering. The separation of the coherent scattering from the Compton scattering is essential for the study of materials containing light elements like the conjugated polymers. For example, in polyaniline at $2\theta = 60°$ the intensity of the Compton scattering is about 3 times larger than that of the coherent scattering. The high resolution of the detector allows the separation of the Kβ coherent scattering from the Kα scattering. However, for large θ the Kβ Compton scattering mixes with the Kα coherent scattering, which may cause some discrepancies in the record of Kα data. Although the use of Kβ radiation is preferable for separation of Compton scattering, we have also used the Kα radiation because of its stronger intensity.

(ii) Theoretical Background and Method of Analysis. Only the coherent part of the diffracted intensity $I_c(K)$ is used in the analysis of the order in amorphous structures ($K = (4\pi \sin \theta)/\lambda$ is the scattering vector, as a function of the Bragg angle θ). The incoherent diffracted intensity has been eliminated by the method outlined above. For a monoatomic isotropic amorphous material, which is nearly the case of polyaniline emeraldine base ($C_{24}H_{18}N_4$), because the carbon and nitrogen atoms have very similar form factors and the scattering by the hydrogen atoms is negligible, the interference function $J(K)$ is defined by

$$J(K) = \frac{I_c(K)}{Nf(K)^2} \tag{1}$$

Here N is the total number of diffracting atoms of form factor $f(K)$. $J(K)$ can be expressed in the Debye approximation under the form[1,25]

$$J(K) = 1 + \int_0^\infty 4\pi r^2[\rho(r) - \rho_0] \frac{\sin Kr}{Kr} dr \tag{2}$$

where $\rho(r)$ is the atomic density and where $\rho_0^{-1} = v$ is the mean atomic volume. If $P(r) = \rho(r)/\rho_0$, the probability of finding an atom at the distance r from a reference atom, is introduced, it

is easy to show, by defining the reduced radial distribution function

$$W(r) = r(P(r) - 1) \tag{3}$$

that eq 2 can be rewritten as

$$F(K) = K[J(K) - 1] = 4\pi\rho_0 \int_0^\infty W(r) \sin Kr \, dr \tag{4}$$

Equation 5 defines a quantity $F(K)$ called the reduced interference function related to $W(r)$ by Fourier transformation

$$W(r) = (2\pi^2\rho_0)^{-1} \int_0^\infty F(K) \sin Kr \, dK \tag{5}$$

Equation 5 is the fundamental equation allowing one to obtain $W(r)$ from the coherent diffracted intensity $I_c(K)$ through the reduced interference function $F(K)$. Experimentally $I_c(K)$ is measured between a minimum (K_m) and a maximum (K_M) wave vector. The truncation of the Fourier transform to the (K_m - K_M) region introduces a broadening of the peaks of $W(r)$ and extraneous oscillations, known as termination ripples, primarily in the vicinity of the first position–position correlation peak.[26] Another important point concerns the normalization of $J(K)$. This is done by noticing that below the first interatomic distance, where $P(r) = 0$, $W(r)$ must have a slope of -1.

At the first interatomic distance and beyond it, position–position correlations lead to oscillations of $P(r)$ and thus, from eq 3, to oscillations of $W(r)$. From the maxima (r_{max}) of these oscillations the average distances to the nth neighbors (d_n) can be obtained. Also, when the peaks of oscillation are well-defined, the average coordination number Z_n to the nth nearest-neighbor can be obtained by integration according to the expression

$$Z_n = \int_{\text{peak } n} 4\pi r^2 \rho(r) \, dr = 4\pi\rho_0 \int_{\text{peak } n} r^2 \left[\frac{W(r)}{r} + 1\right] dr \tag{6}$$

Data obtained with Ag Kα and Ag Kβ characteristic radiations between K_m and K_M, approximately equal to 0.5 and 15 Å^{-1}, respectively, were both analyzed in our study of polyaniline. Practically the same functions $W(r)$ were found for both wavelengths. In particular, the peak positions (r_{max}) of $W(r)$ are reproducible within 0.1 Å (low r values) to 0.2 Å (large r values).

(b) Preparation of Polyaniline Films. The study has been performed on three unstretched films of polyaniline each of lateral dimensions 10 × 10 mm^2 and 60 μm thick. These films originated from the same preparation. First a large EB-II film was prepared from NMP solution according to the procedure described in refs 22 and 23. About $^1/_3$ of this film was kept, forming sample A. Then the remaining part of the film was converted into ES-II (with [Cl]/[N] ≈ 0.5) by equilibration of the EB-II film in a HCl solution of pH = 0. Half of it was saved, constituting sample B. Finally the remaining part of the film was dedoped by washing with 1 M NH_4OH. It forms sample C.

Guinier patterns used to test the X-ray diffraction of these samples showed the three films to be amorphous. After the long X-ray exposure required to record the interference functions, these samples were checked once more with the Guinier camera. Their X-ray patterns did not show any structural evolution. It should be noticed that our observation of quasi amorphous EB-II and ES-II films contrasts with earlier reports[9,11] of crystallinity in unstretched EB-II and ES-II films. These differences are likely due to variations in preparation conditions. However, according to our own investigations, the completely amorphous state seems to be the most frequent in type II unstretched films or fibers: seven EB-II samples out of nine and two ES-II samples out of four were found to be amorphous.

III. Results

(a) Reduced Interference Functions $F(K)$. Figures 3–5 display the reduced interference functions $F(K)$ of samples A–C. Figure 3 was obtained with Ag Kα and Figures 4 and 5 with Ag Kβ. Similar diffraction patterns are obtained with the complementary radiation. A comparison of these $F(K)$ already shows that the K_{max} position of the first peak differs between the three samples investigated. In sample A it occurs at ~1.4 Å^{-1}, which corresponds to approximately the position of the (110) reflection of the crystalline part of EB-II samples investigated in refs 9 and 11. In sample B this peak has shifted to a larger wave vector of ~1.8 Å^{-1}, which is the postion of the (200) reflection of the crystalline part of ES-II.[11] In dedoped sample C the first peak shifts back but does not recover the position observed in the undoped sample A. It is observed at ~1.6 Å^{-1}, an intermediate wave vector between those corresponding to the first peak in samples A and B. More generally the reduced interference function

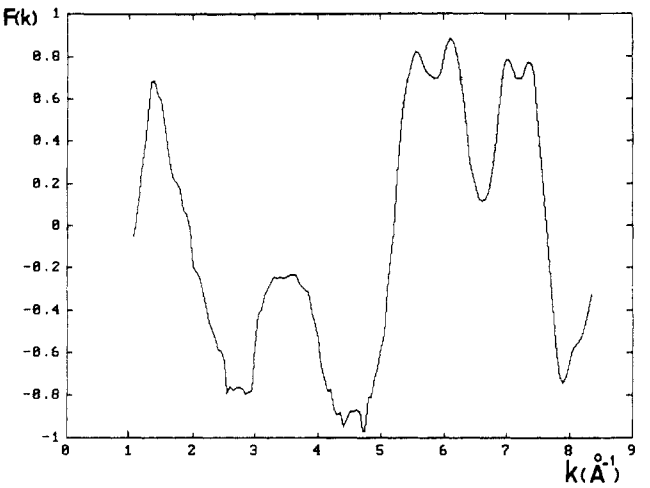

Figure 3. Reduced interference function $F(K)$ derived from the measured intensity (Ag Kα) of undoped polyaniline (sample A).

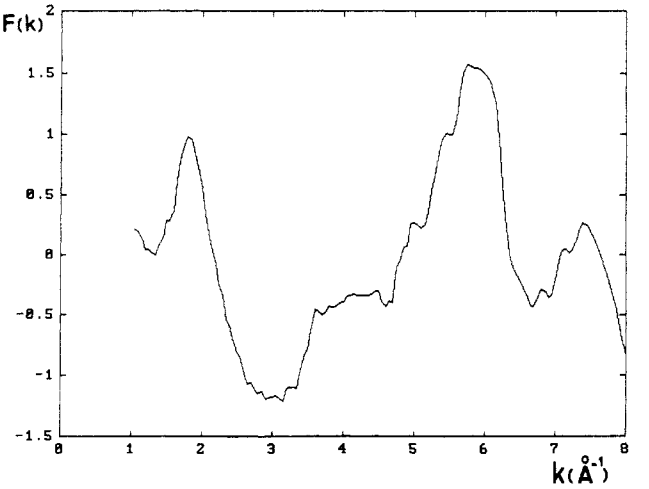

Figure 4. Reduced interference function $F(K)$ derived from the measured intensity (Ag Kβ) of HCl-doped polyaniline (sample B).

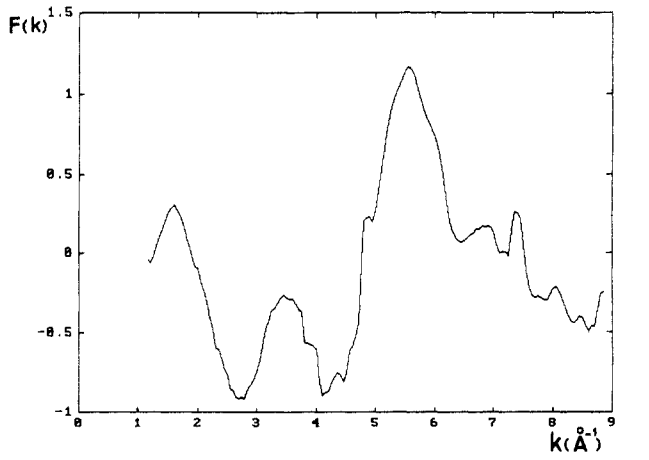

Figure 5. Reduced interference function $F(K)$ derived from the measured intensity (Ag Kβ) of dedoped polyaniline (sample C).

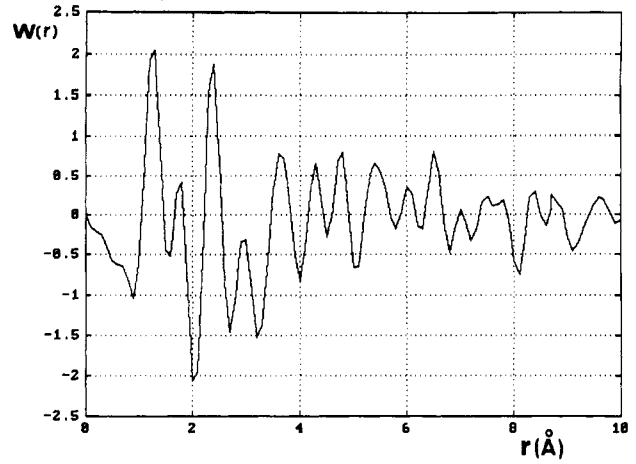

Figure 6. Reduced radial distribution function $W(r)$ of sample A derived from the Fourier transform of $F(K)$ shown in Figure 3.

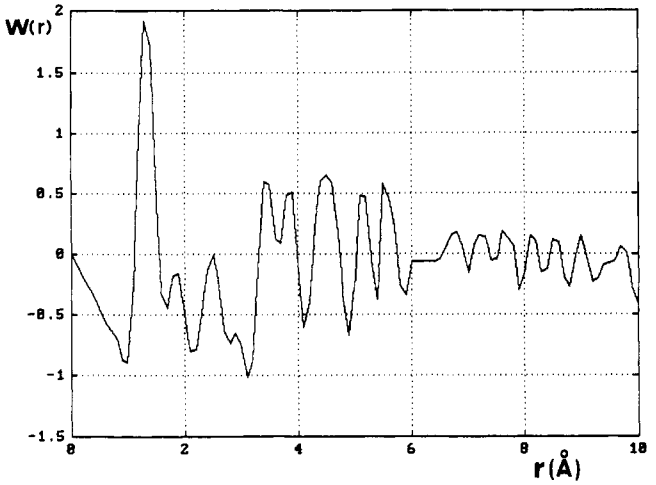

Figure 7. Reduced radial distribution function $W(r)$ of sample B derived from the Fourier transform of $F(K)$ shown in Figure 4.

$F(K)$ of sample C (Figure 5) differs from those of both samples A (Figure 3) and B (Figure 4).

(b) Reduced Radial Distribution Functions $W(r)$. In order to obtain more information on the amorphous structure of the various forms of polyaniline, the reduced interference functions $F(K)$ obtained with both Ag Kα and Ag Kβ were analyzed by Fourier transform as described in section IIa.ii. Figures 6–8 display the reduced radial distribution functions obtained from the $F(K)$ respectively shown in Figures 3–5. Clear oscillations of $W(r)$ are observed for samples A and B. These oscillations are substantially damped for $r > 3.4$ Å in sample C. Table I gives for each sample a list of the distances r_{max} at which $W(r)$ shows a maximum. We limit r_{max} to 7 Å to only include first- and second-nearest-neighbor chains. This table will be discussed in the next section. It is interesting to note that the r_{max} of sample C are intermediate between the r_{max} of samples A and B.

The $W(r)$ of sample B (HCl-doped polyaniline corresponding to the approximate chemical formula $C_{12}H_{10}N_2Cl$) has been obtained, as for samples A and C, assuming a pseudo monoatomic amorphous solid. The analysis of $F(K)$ diffracted from sample B thus ignores the presence of Cl atoms between the polymeric chains. This can be justified by the similarity displayed by the $W(r)$ for the three samples investigated, showing that the main position–position correlations involve atoms belonging to the covalently bonded polymer chains. The relative unimportance of the Cl contribution is reasonable in light of the expected large randomness in the placement of the Cl^- ions; also the Cl^- have only 16% of the total number of electrons.

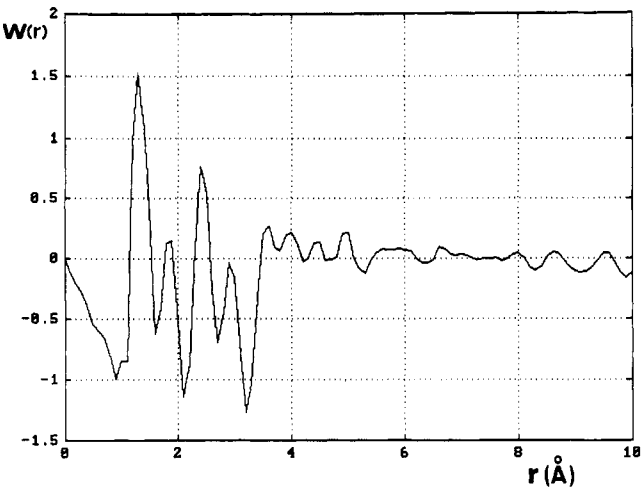

Figure 8. Reduced radial distribution function $W(r)$ of sample C derived from the Fourier transform of $F(K)$ shown in Figure 5.

Table I
Position of the First Maxima (in Å), r_{max}, of $W(r)$ of Amorphous Polyaniline Shown in Figures 6–8 for Samples A–C, Respectively

undoped (sample A)	HCl doped (sample B)	dedoped (sample C)
1.2_5	1.3	1.3
1.8	1.8_5	1.8_5
2.4	2.5	2.4
2.9_5	2.9	2.9
3.6_5	3.4_5	3.6
	3.8_5	3.9_5
4.3	4.5	4.4_5
4.8	5.1_5	4.9_5
5.4	5.6_5	
6.0_5		~5.8
6.5	~6.2	
	6.75	6.65
7.0		

IV. Analysis of the Reduced Radial Distribution Functions

For an amorphous polymer the probability $P(r)$ related by eq 3 to the reduced radial distribution function $W(r)$ can be decomposed into the sum of an intrachain probability $P_I(r)$ and of an interchain one $P_E(r)$. $P_I(r)$ gives information on correlations between atoms covalently bonded in a given polymeric chain while $P_E(r)$ gives information on the chain packing. We consider these two contributions successively.

(a) Intrachain Radial Distribution Function. In order to find the characteristic distances of the polyaniline chain, it is drawn as a first approximation, on a graphitic lattice as shown by Figure 9. This approximation ignores the difference between benzenoid (75% of the carbon) and quinoid (25% of the carbon) and sets the C–N and C=N distances to the same value. We assume also that all the bond angles (the C–N–C zigzag angle δ in particular) are of $2\pi/3$ and that the phenyl ring is not tilted with respect to the plane defined by the nitrogen atoms ($\Phi = 0$). Thus there is only one free parameter, the first-neighbor distance d. Table II gives the expression of the nth neighbor distances for this case, d_n^I, for n up to 10. In this table these distances are calculated using $d = 1.375$ Å, the average first-neighbor atomic distance according to

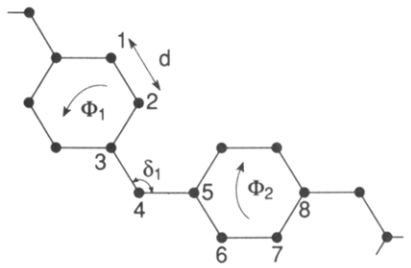

Figure 9. Schematic drawing of an ideal polyaniline chain on a graphitic lattice. This figure defines also the two main angular degrees of freedom δ (zigzag angle) and Φ (ring torsion angle) of the chain. The atom labeling is used in Table II.

Table II
***n*th Neighbor Distances d_n between Atoms of a Polyaniline Backbone Drawn on a Graphitic Lattice up to $n = 10$[a]**

	d_n^I			$Z_n^{I''}$		
n	anal.	calcd (Å)	$Z_n^{I'}$	(δ_1)	(δ_1, Φ_1)	(Φ_1, δ, Φ_2)
1	1–2:d	1.375	16/7	0	0	0
2	1–3:$d\sqrt{3}$	2.38	20/7	2/7	0	2/7
3	2–5:2d	2.75	6/7	0	4/7	0
4	1–4:$d\sqrt{7}$	3.64	8/7	0	4/7	4/7
5	1–5:3d	4.12	4/7	0	4/7	4/7
6	2–8:2$d\sqrt{3}$	4.76	0	0	8/7	4/7
7	2–7:$d\sqrt{13}$	4.96	0	4/7	0	4/7
8	1–6:4d	5.50	2/7	0	0	4/7
9	1–8:$d\sqrt{19}$	5.99	0	0	8/7	4/7
10	1–7:$d\sqrt{21}$	6.30	0	4/7	4/7	4/7

[a] All the first-neighbor distances d are the same, and all the angles are 120°. This table gives also the average coordination Z_n^I of an atom to its nth neighbors. This quantity has been split into two components depending upon the linked atoms being in the same repeat unit ($Z_n^{I'}$) or in neighboring ones ($Z_n^{I''}$). In the last case the $Z_n^{I''}$ have been classified according to the number of degrees of freedom that may modify these distance (δ, zigzag angle, or Φ, ring tilt angle). Notation and atom labeling are defined by Figure 9.

the structural refinements of salts of "tetramers" and "dimers" of aniline.[24] A comparison of Tables I and II shows that such a simple model can account (within 0.2 Å) for the position of all the maxima of $W(r)$ observed in undoped polyaniline (sample A) except the one found at 1.8 Å which will be considered later. However, such an agreement must be treated with caution because a sizable interchain contribution is generally expected, and even for the intrachain contribution a distribution of d, deviations of δ and intraring bond angles from 120°, and variation of Φ from 0° certainly occur.

In the amorphous state there is certainly a distribution of δ and of Φ, the two main degrees of freedom of the polyaniline chain. Because of that we have separated in Table II the average coordination number to the nth neighboring atoms Z_n^I into several components according to the influence of δ and Φ on the distance d_n^I. To illustrate these effects, we have calculated in the case of the EB-II "crystalline" structure, for which $\delta = 130°$ and $\Phi = 30°$,[11] the distribution of intrachain distances d_n^I. The corresponding histogram, Z_n^I as a function of d_n^I, is given by the black columns in Figure 10. As expected, δ shifts significantly some of the d_n^I distances, while Φ increases mainly the shortest distances with respect to the ones calculated in Table II.

The peaks of $W(r)$ observed below about 3.4 Å, a typical interchain contact distance, are due to atoms covalently bonded within a polymer chain. Those occurring at about the same r_{max} of 1.3, 2.4, and 2.9 Å in samples A–C (Table I) correspond to the intrachain separation between first, second, and third neighbors.

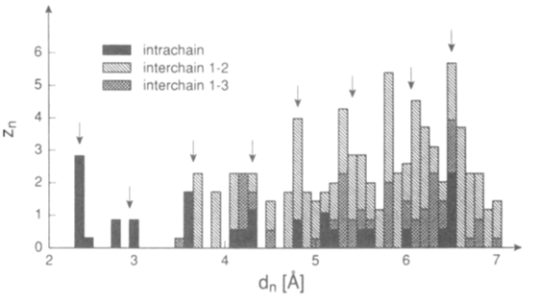

Figure 10. Average atomic coordination number Z_n as a function of the interatomic distance d_n for the EB-II crystalline structure of polyaniline. The distances have been regrouped by steps of 0.1 Å. Z_n has been separated into intrachain and first- and second-neighbor interchain contributions. The lattice parameters used for this histogram are those given in Figure 1 with $\Phi = 30°$. Observed r_{max} of sample A are shown by arrows.

We have used the expression in eq 6 with a mean atomic volume $v = 16$ Å^3 ($^1/_{28}$ of 450 Å^3: the unit cell volume of emeraldine base[9,11]) to obtain the Z_n^I from these first peaks in the case of sample A. The peak centered at 1.25 Å leads to a coordination number of 1.3 which is much less than the expected value $^{16}/_7$. However, this value is nearly recovered if we add to 1.3 the coordination number corresponding to the peak centered at 1.8 Å: 0.8. The same result is obtained by integration of the two first peaks of $W(r)$ of samples B and C. There is however no chemical reason for which a fraction of the first atomic distances could be as long as 1.8 Å. Thus the splitting of the first correlation peak is more likely caused by an artifact due either to imperfect Compton scattering corrections for large 2θ angles or to termination ripples caused by the limited range of 2θ values scanned in recording $I(K)$. In particular, termination effects are known to introduce, by Fourier transform, spurious peaks in the near vicinity of the first correlation peak.[26] In our case these artifacts do not perturb significantly the distribution function for larger values of r, as proven by the accuracy of the informations which can be extracted from the second correlation peak of sample A. This peak, which is centered at the right r spacing (2.4 Å), gives, by integration, a coordination number of 3.1, which corresponds to $^{22}/_7$, the sum of the Z_n of the peaks at 2.4 and 2.5 Å in Figure 10. The coordination number corresponding to the peak centered at 2.95 Å is more inaccurate due to the overlap with the broad peak centered at 3.65 Å. Nevertheless, this number can be estimated at 1.5 (±0.3) in good agreement with $^{12}/_7$, the sum, of the Z_n of the peaks at 2.8 and 3 Å in Figure 10.

A comparison of Figures 6 and 7 shows, in the case of doped polyaniline (sample B), a broadening and a large decrease of the intensity at the maximum for the peak centered at 2.5 Å and a near vanishing of the peak centered at 2.9 Å. Such an effect can be explained by a wider distribution of distance in $P_1(r)$. As the peaks observed at 1.3 and 1.85 Å and corresponding to first-neighbour distances remain nearly unchanged, the broadening of $P_1(r)$ can be caused by a larger distribution of angular variables (i.e., intraring angular deformation, and possibly wider spreading of δ and Φ). Figure 8 shows that upon dedoping the polyaniline the peaks centered at 2.4 and 2.9 Å have nearly recovered the intensity and shape they had in undoped polyaniline (Figure 6). This means that some intrachain angular variables, like the intraring angles, behave reversibly with doping.

For distances larger than 3.4 Å interchain contributions must be explicitly considered to account for the experimental $W(r)$. This is the object of the next part.

Table III
Expression of the Interchain Distances d_n^E of Two Ideal Zigzag Segments of Polyaniline in Close Contact on Top of Each Other and Calculation of These Distances with the ES-II Parameters $a' = a/2 = 3.5$ Å and $c' = c/2 = 5.2$ Å and the Average First Neighbor Distance $d = 1.4$ Å[a]

d_n^E anal.	d_n^E calcd (Å)	r_{max} (Å)
a'	3.5	3.45
$\sqrt{a'^2 + d^2}$	3.8	3.85
$\sqrt{a'^2 + 3d^2}$	4.3	4.5
$\sqrt{a'^2 + 4d^2}$	4.5	
$\sqrt{a'^2 + 7d^2}$	5.1	5.15
$\sqrt{a'^2 + 9d^2}$	5.5	5.65
$\sqrt{a'^2 + c'^2}$	6.3	~6.2
$\sqrt{a'^2 + 16d^2}$	6.6	6.75

[a] The last column allows us to compare these distances with the experimental r_{max} of Table I.

(b) Interchain Radial Distribution Function. Interchain correlations involve interatomic distances larger than the sum of van der Waals radii of atoms belonging to neighboring polymer chains. In the case of polyaniline this critical distance is ~3.4 Å (van der Waals diameter of a C atom, d_c, or thickness of a phenyl ring, d_φ)[27] according to the structures proposed for the crystalline regions of EB-II (Figure 1) and ES-II (Figure 2). In the following we compare the most probable interchain distances (i.e., r_{max} of $W(r)$) of samples A and B with those expected from the "crystalline" EB-II and ES-II structures, respectively.

Because the phenyl rings are titled by Φ, there is a large distribution of interchain distances, d_n^E, for $r > d_c$ in the EB-II structure. Thus, in order to compare more easily the d_n^E with the $W(r)$ data, we have regrouped in the same column in Figure 10 all the calculated d_n^E situated within less than ±0.05 Å of the central value. One column is defined every 0.1 Å, the accuracy in our r_{max} determination. The d_n^E distances are calculated according to the lattice parameters given by Figure 1 and obtained from crystalline EB-II induced by 4-fold stretching a film with the same (amorphous) diffraction pattern as sample A and for Φ = 30° according to ref 11. In Figure 10 we have separated the first-neighboring chain (interchain 1–2) and the second-neighboring chain (interchain 1–3) distances d_n^E (third-neighboring chains which contribute to $r_{max} >$ 7 Å are not considered here). We have also included, for a meaningful comparison with the experimental data, the intrachain contribution considered in section IVa. The number of distances is expressed in terms of an average atomic coordination number Z_n. Figure 10 shows that all the r_{max} observed in sample A (arrows) correspond within less than 0.1 Å to the d_n for which a maximum can be defined in the Z_n histogram. There is however an additional maximum at about 5.8 Å which is not clearly observed. This peak disappears and the agreement with the experimental r_{max} is improved if in the histogram of Figure 10 the interchain 1–3 distances are increased by 0.1 Å from their value in crystalline EB-II. Such a shift together with a spread of average distances to the second-neighbor chains can be reasonably expected in an amorphous state.

The calculation of interchain distances d_n^E can be performed analytically in the case of the ES-II structure because, as shown by Figure 2, the rings are packed on top of each other. Table III gives the expression for the first eight interchain distances d_n^E, as well as their calculation for reasonable values of the parameters defined in the table (distances to second-neighboring chains which contribute to $r_{max} > 7$ Å are not considered here). The calculated d_n^E account quite well for the r_{max} observed in sample B. (Because of the broadening of the intrachain distribution of distances observed for small r (see section IVa), the oscillations of $W(r)$ observed for $r > d\varphi$ are mostly caused by the interchain correlations.) The agreement shows again that the local structure of amorphous HCl-doped polyaniline is close to that of the crystalline part of ES-II. However, Figure 7 shows that there is a sizable damping of the oscillations of $W(r)$ for $r > 6$ Å. This means that these is a substantial loss of correlations beyond first-neighbor polyaniline rings in close contact.

$W(r)$ of sample C shows vanishing by small oscillations for $r > 3.4$ Å (Figure 6). The most reasonable interpretation of this behavior is the presence of a wider distribution of distances d_n^E and d_n^I than for samples A and B. This can be understood if after dedoping there is a very large distribution of interchain local order between those of ES-II and EB-II, with a broad maximum of the distribution for intermediate local orders in agreement with finding the weak maximum of $W(r)$ at r_{max} intermediate between those of amorphous ES-II and EB-II (see Table I). Such an intermediate interchain local order is also corroborated by the observation of a first peak of $F(K)$ in dedoped polyaniline at a $K_{max} \sim 1.6$ Å^{-1} which is the average between those of ES-II (1.8 Å^{-1}) and of EB-II (1.4 Å^{-1}). With an increase in the mean interchain distance from ES-II to EB-II the ring tilt angle Φ will increase, causing, together with a variation of δ, also a large distribution of intrachain distances d_n^I.

V. Implications for Physical and Chemical Phenomena

An important result of the present structural study is that amorphous undoped and HCl-doped polyaniline of type II have a local chain array resembling that exhibited by the EB-II and ES-II crystalline structures, respectively. The observed and calculated interchain distances in the amorphous and crystalline structures, respectively, agree quite well within 0.1 Å for $r < 7$ Å. In amorphous EB-II polyaniline there is a substantial local order on a scale of distances up to ~10 Å (beyond second-nearest-neighbor chain distances). In amorphous ES-II substantial position–position correlations are observed up to ~6 Å (first-nearest-neighbor chain distances). These scales of distances are about 1 order of magnitude smaller than the size of crystalline domains observed in EB-II and ES-II powders (~50 Å) and EB-II THF-extracted powders (~100 Å).[11] In amorphous polyaniline there is a poor chain order probably because of the presence of numerous conformational defects of the polymer. However, with similar interchain correlations for crystalline and amorphous ES-II, it is not surprising that amorphous polyaniline films could be converted into partly crystalline polyaniline upon stretching. Crystallinity is certainly induced in regions where stresses are able to transform the conformational defects. In accordance with previous reports,[28,29] we have observed during this study that a 4-fold stretching of a film analogous to sample A gives rise to some well-defined reflections at d spacings of 4.64 and 3.86 Å in the equatorial direction and of 5 Å in the meridional one, which correspond to the (110), (200), and (002) reflections of crystalline EB-II,[11] respectively (the distances given in Figure 1 are obtained from this measurement). In summary the amorphous and crystalline regions of polyaniline have the same local order. They differ only in the

range of spatial correlations. Hence, the boundary between crystalline and amorphous regions is not really distinct. Such a result is expected when polymer chains are not too strongly disordered. However, this conclusion certainly does not hold for polymers with many imperfections, especially when amorphous regions are nucleated by cross-linking between chains. In this case a description in terms of two-phase structure is more appropriate.[1]

A second important result of this investigation is the structural proof of a memory effect in the doping–dedoping process of polyaniline. The $r > 3.5$ Å part of $W(r)$ obtained for sample C shows that upon dedoping ES-II the chains do not recover their local position of the EB-II structure.[30] Most of the chains adopt a local array intermediate between those of the ES-II and EB-II structures. This explains the previous observation[11] that dedoped amorphous EB-II recovers the ES-II structural type, not the ES-I one, upon redoping.

These studies demonstrate the importance of sample history in evaluating the electronic properties of polyanilines. For example, the presence of at least 17 orders of magnitude of time scales of response that occur in the polyanilines upon photoexcitation (from 10^{-13} s[31] to $> 10^{4}$ s[18]) and the existence of very long-lived photoinduced changes in spectra reflect the changes in conformation of polymer chains upon photoexcitation of charge.[18] This long-lived optical absorption has led to the proposal of utilizing polyanilines as a medium for erasable optical information storage.[32] Sample history also plays a role in electrochemical cycling where hysteresis has been reported[15,16] that has been proposed to originate from an electronic effect.[15] However, the experimental results reported here demonstrate that upon doping and dedoping the polymer structure does not immediately relax back to its original form. Hence, polymer chain structural relaxation may play an important role in the memory effect that occurs in electrochemical cycling.

The reported selectivity of polyaniline membranes for the diffusion of gases and the change of this selectivity upon doping and dedoping of the membranes[17] reflect the important role of order within the amorphous polymer structures. In particular, the enhanced permeabilities of gases and increased selectivity noted for polyaniline (EB-II) films upon doping and dedoping may reflect the fact that the rings of the EB-II chains are more nearly planar after doping and dedoping, allowing easier transmission of the gas molecules through the polymer film. Hence, a doping and dedoping cycle is a useful way to control the internal morphology of this polymer system. The improved selectivity for particular gases that occurs upon partial redoping[17] may be related to the elimination of the most open channels within the polymer through protonation and the concomitant insertion of a Cl^- ion in the channel. The protonation is expected to occur most rapidly and most preferentially through regions that are most open in the structure and hence would block channels that would otherwise be open for rapid gas diffusion.

The effect of disorder within the ES-II structure on charge transport has been the subject of extensive study.[13] Recent results indicate that the conduction electrons are three-dimensionally delocalized within the three-dimensionally coherent crystalline regions; however, the dc conductivity remains dominated by quasi-one-dimensional variable range hopping which occurs within the amorphous region. The lack of sufficient coherence, both within the chain and between the chains, is the essential cause of the charge localization in the amorphous regions.[13] The disorder characterized during this diffraction study suggests that the conditions necessary for applicability of the random-dimer model of Wu and Phillips are unlikely to be present in the amorphous regions.[33] Because the site energies will vary from location to location due to the disorder, the rigorous conditions necessary for the random-dimer model will unlikely be fulfilled.

VI. Summary

We introduced here a nondispersive X-ray technique for application in amorphography of polymers, using this technique to obtain for the first time the radial distribution function of three different amorphous states of electronic polymers of the polyaniline family. Position–position correlations have been deduced from the record of good quality interference functions where the use of a non-energy-dispersive X-ray diffraction technique has facilitated the important background corrections. Improvement in the quality of the data is planned in the near future by an extension of the 2θ range of measurement on samples of a larger volume. This study and earlier ones show that there is a wide range of order and coherence lengths in polyaniline. This order is dependent upon preparation conditions, doping, dedoping, etc. These changes in order have important ramifications for photoinduced optical phenomena, conductivity, electrochemical response, and even gas diffusion selectivity. The future determination of order in other polymer systems will provide further insight into the control of the science and technology of conducting polymers.

Acknowledgment. This work was supported in part by the Defense Advanced Research Project Agency through a contact monitored by the U.S. Office of Naval Research, NSF International Grant No. 9016586 and by an "Action Incitative CNRS-NSF". Laboratoire de Physique des Solides is associated to the "Centre National de la Recherche Scientifique".

References and Notes

(1) Kakudo, M.; Kasai, N. *X-Ray Diffraction by Polymers*; Kodanshaltd, Tokyo, and Elsevier Publishing Co. Amsterdam, The Netherlands, 1972.
(2) Akaishi, T.; Miyasaka, K.; Ishikawa, K.; Shirakawa, H.; Ikeda, S. *J. Polym. Sci., Polym. Phys. Ed.* **1980**, *18*, 745.
(3) Haberkorn, H.; Naarmann, H.; Penzien, K.; Schlag, J.; Simak, P. *Synth. Met.* **1982**, *5*, 51.
(4) Robin, P.; Pouget, J. P.; Comes, R.; Gibson, H. W.; Epstein, A. J. *Polymer* **1983**, *24*, 1558; *J. Phys. (Paris)* **1983**, *44*, C3-87.
(5) Baughman, R. H.; Hsu, S. L.; Pezi, G. P.; Signorelli, A. J. *J. Chem. Phys.* **1978**, *68*, 5405. Baughman, R. H.; Murthy, N. S.; Miller, G. G. *J. Chem. Phys.* **1983**, *79*, 515.
(6) Pouget, J. P. *Solid State Sci. (Springer)* **1985**, *63*, 26.
(7) See, for example: Proceedings of the International Conference on the Science and Technology of Synthetic Metals, Tubingen, Germany, Sept 1990 (*Synth. Met.* **1991**, *41–43*); Santa Fe, NM, June 1988 (*Synth. Met.* **1989**, *27–29*).
(8) Fosong, W.; Jinsong, T.; Lixiang, W.; Hongfang, Z.; Zhishen, M. *Mol. Cryst. Liq. Cryst.* **1988**, *160*, 175.
(9) Jozefowicz, M. E.; Laversanne, R.; Javadi, H. H. S.; Epstein, A. J.; Pouget, J. P.; Tang, X.; MacDiarmid, A. G. *Phys. Rev. B* **1989**, *39*, 12958.
(10) Moon, Y. B.; Cao, Y.; Smith, P.; Heeger, A. J. *Polym. Commun.* **1989**, *30*, 196.
(11) Pouget, J. P.; Jozefowicz, M. E.; Epstein, A. J.; Tang, X.; MacDiarmid, A. G. *Macromolecules* **1991**, *24*, 779.
(12) Jozefowicz, M. E.; Epstein, A. J.; Pouget, J. P.; Masters, J. G.; Ray, A.; Sun, Y.; Tang, X.; MacDiarmid, A. G. *Synth. Met.* **1991**, *41*, 723.
(13) Wang, Z. H.; Li, C.; Epstein, A. J.; Scherr, E. M.; MacDiarmid, A. G. *Phys. Rev. Lett.* **1991**, *66*, 1745. Wang, Z. H.; Scherr, E. M.; MacDiarmid, A. G.; Epstein, A. J. *Phys. Rev. B* **1992**, *45*, 4190.
(14) Wang, Z. H.; Javadi, H. H. S.; Ray, A.; MacDiarmid, A. G.; Epstein, A. J. *Phys. Rev. B* **1990**, *42*, 5411. Wang, Z. H.; Ray, A.; MacDiarmid, A. G.; Epstein, A. J. *Phys. Rev. B* **1991**, *43*, 4373.

(15) Villeret, B.; Nechtschein, M. *Phys. Rev. Lett.* **1989**, *63*, 1285.
(16) Huang, W. S.; Humphrey, B. D.; MacDiarmid, A. G. *J. Chem. Soc., Faraday Trans. 1* **1986**, *82*, 2385.
(17) Anderson, M. R.; Mattes, B. R.; Reiss, H.; Kaner, R. B. *Synth. Met.* **1991**, *41*, 1151.
(18) McCall, R. P.; Ginder, J. M., Leng, J. M.; Ye, H.; Manohar, S. K.; Masters, J. G.; Asturias, G. E.; MacDiarmid, A. G.; Epstein, A. J. *Phys. Rev.* **1990**, *B41*, 5202. McCall, R. P.; Ginder, J. M.; Leng, J. M.; Coplin, K. A.; Ye, H. J.; Epstein, A. J.; Asturias, G. E.; Manohar, S. K.; Scherr, E. M.; Sun, Y.; MacDiarmid, A. G. *Synth. Met.* **1991**, *41*, 1329.
(19) Cromack, K.; Epstein, A. J.; Masters, J.; Sun, Y.; MacDiarmid, A. G. *Synth. Met.* **1991**, *41*, 641.
(20) Ginder, J. M.; Epstein, A. J. *Phys. Rev. B* **1990**, *41*, 10674.
(21) Laridjani, M.; Sadoc, J. F. *J. Phys. (Fr.)* **1981**, *42*, 1293.
(22) Angelopoulos, M.; Asturias, G. E.; Ermer, S. P.; Ray, A.; Scherr, E. M.; MacDiarmid, A. G.; Akhtar, M.; Kiss, Z.; Epstein, A. J. *Mol. Cryst. Liq. Cryst.* **1988**, *160*, 383.
(23) MacDiarmid, A. G.; Epstein, A. J. *Faraday Discuss. Chem. Soc.* **1989**, *88*, 317.
(24) Baughman, R. H.; Wolf, J. P.; Eckhardt, H.; Shacklette, L. W. *Synth. Met.* **1988**, *25*, 121.
(25) Guinier, A. *Théorie et Technique de la Radiocristallographie*, 3rd ed.; Dunod: Paris, 1964.
(26) Kaplow, R.; Strong, S. L.; Averbach, B. L. *Phys. Rev.* **1965**, *138*, A1336.
(27) Pauling, L. *The Nature of the Chemical Bond*, 3rd ed.; Cornwell University Press: Ithaca, NY, 1973.
(28) Cromack, K. R.; Jozefowicz, M. F.; Ginder, J. M.; Epstein, A. J.; McCall, R. P.; Du, G.; Leng, J. P.; Kim, K.; Li, C.; Wang, Z. H., Druy, M. A.; Glatkowski, P. J.; Scherr, E. M.; MacDiarmid, A. G. *Macromolecules* **1991**, *24*, 4157.
(29) Fischer, J. E.; Tang, X.; Scherr, E. M.; Cajipe, V. B.; MacDiarmid, A. G. *Synth. Met.* **1991**, *41*, 661.
(30) Similar to the situation for amorphous polyanilines, it has been previously reported that a degradation of the crystalline structure of polyacetylene occurs upon doping and dedoping with ClO_4^-. This is probably due to a distribution of chain arrays between those of the trans $(CH)_x$ and those of the intercalated $[CH(ClO_4)_y]_x$ structures upon dedoping. Pouget, J. P.; Pouxviel, J. C.; Robin, P.; Comes, R.; Begin, D.; Billaud, D.; Feldblum, A.; Gibson, H. W.; Epstein, A. J. *Mol. Cryst. Liq. Cryst.* **1985**, *117*, 5.
(31) Vardeny, Z.; Epstein, A. J.; MacDiarmid, A. G., to be published.
(32) McCall, R. P.; Ginder, J. M.; Leng, J. M.; Coplin, K. A.; Ye, H. J.; Epstein, A. J.; Asturias, G. E.; Manohar, S. K.; Masters, J. G.; Scherr, E. M.; Sun, Y.; MacDiarmid, A. G. *Synth. Met.* **1991**, *41–43*, 1329.
(33) Wu, H. L.; Phillips, P. *Phys. Rev. Lett.* **1991**, *66*, 1366. Phillips, P.; Wu, H. L. *Science* **1991**, *252*, 1805.
(34) There are also significant differences of local order between amorphous EB-II and EB-I. See: Laridjani, M.; Pouget, J. P.; MacDiarmid, A. G.; Epstein, A. J. *J. Phys. I Fr.* **1992**, *2*, June issue.

Registry No. Polyaniline, 25233-30-1.